AIAA JOURNAL
Vol. 32, No. 8, August 1994

Staggered Finite Volume Scheme for Solving Cascade Flow with a k-ω Turbulence Model

Fieng Liu* and Xiaoqing Zheng†
University of California, Irvine, Irvine, California 92715

A k-ω turbulence model by Wilcox is applied to cascade flow calculations. A staggered finite volume scheme is proposed to solve the compressible Reynolds-averaged Navier-Stokes equations and the k-ω model equations. The Navier-Stokes equations are solved with a cell-centered scheme, whereas the k-ω equations are solved on staggered control volumes with k and ω defined at the cell vertices of the original grid. By use of this combination of the cell-centered and cell-vertex schemes, the method maintains a small stencil for all diffusion terms and closely couples the Navier-Stokes and k-ω equations. This enhances the stability of the numerical computation. Numerical results compare well with empirical correlations for flat-plate flow. Application to cascade flow was conducted at design and off-design conditions. Good agreement with experimental data was achieved. The proposed discretization is applicable to other one- or two-equation turbulence models.

I. Introduction

THE development of efficient numerical methods and powerful computers has enabled us to solve the Reynolds-averaged Navier-Stokes equations for practical aerodynamic applications.[1-3] However, the accuracy of the computation depends heavily on the performance of turbulence models. The requirement for reliable turbulence models has become increasingly important in the prediction of complex flows of practical interest.

Among the turbulence models used today, two-equation eddy-viscosity models appear to be favored because they incorporate substantially more turbulence physics and less ad hoc empiricism than algebraic models while avoiding difficulties in numerical implementation and excessive computational cost with other more complex models. Among two-equation eddy-viscosity models, the k-ε model by Launder and Spalding[4] is probably the most popular. With the use of wall functions, the k-ε model is reasonably well behaved and enjoys moderate success in application to a variety of engineering problems as documented by Launder[5] and Speziale.[6]

One major difficulty with the k-ε model involves its application to near-wall turbulent flows where inaccuracy and numerical stiffness may arise.[7,8] Therefore a number of alternative models have been developed. A most notable alternative model is the k-ω model developed by Wilcox[9,10] It has the advantage that it does not require damping functions in the viscous sublayer. The model equations are mathematically simpler and less stiff near walls. From the point of computational implementation, this model appears especially attractive. Furthermore, it has been designed to achieve more accurate predictions for adverse pressure gradient flows. Wilcox reported superior results over other two-equation models.[9,10] Very encouraging results for separated flows have also been reported by Menter.[11]

The aforementioned advantages offered by the k-ω model are the major motivation for the present application. From the available papers concerning the k-ω model, it is also noted that most studies of the k-ω model have been restricted to solving the boundary-layer equations.[9,10,12] Menter[11] solved the incompressible Reynolds-averaged Navier-Stokes equations, but the computations were started where the flow is already turbulent and the profiles of k and ω were prescribed either from experiments or other models. In practical applications, the precise specification of such boundary conditions is not possible. Usually, only flow parameters at the incoming flow boundary far away from the wall or boundary layer are specified. For instance, in the case of cascade flows, the known variables are the flow angle, stagnation pressure and stagnation temperature at the inlet, and the back pressure at the exit. The behavior of the k-ω model under such practical conditions needs to be determined.

In the present paper, a numerical method is presented to solve the compressible Reynolds-averaged Navier-Stokes equations and the k-ω model equations. A unique feature of this method is that the density ρ, internal energy e, and momentum flux ρu, ρv, and ρw are defined at cell centers, whereas k and ω are defined at cell vertices. Staggered control volumes are used for the Navier-Stokes equations and the k-ω turbulence model equations. This strategy keeps the discretization stencil to a minimum. The production terms in the model equations are obtained at exactly the same locations where the stress tensors in the Navier-Stokes equations are evaluated. Thus, excess averaging can be avoided, and the resulting discrete equations for the Navier-Stokes and k-ω equations are closely coupled. This increases the stability as well as the accuracy of the scheme.

In the following sections we will first outline the basic governing equations including the k-ω turbulence model equations. The numerical method is presented in Sec. III. Section IV shows the computational results for a flat plate and a low-pressure turbine cascade. The flat-plate calculation is used to validate our code. Three operating conditions are computed for the three-dimensional turbine cascade case. Results are compared with experiments and calculations by the Baldwin-Lomax algebraic model.

II. Governing Equations

The governing equations for general compressible turbulent flows with a k-ω turbulence model, as given by Wilcox,[9] can be summarized as follows.

Mass conservation:

$$\frac{\partial \rho}{\partial t} + \frac{\partial}{\partial x_j}(\rho u_j) = 0 \tag{1}$$

Momentum conservation:

$$\frac{\partial}{\partial t}(\rho u_i) + \frac{\partial}{\partial x_j}(\rho u_j u_i) = -\frac{\partial p}{\partial x_i} + \frac{\partial \hat{\tau}_{ji}}{\partial x_j} \tag{2}$$

Presented as AIAA Paper 93-1912 at the AIAA/SAE/ASME/ASEE 29th Joint Propulsion Conference, Monterey, CA, June 28–30, 1993; received July 17, 1993; revision received March 1, 1994; accepted for publication March 6, 1994. Copyright © 1994 by F. Liu and X. Zheng. Published by the American Institute of Aeronautics and Astronautics, Inc., with permission.

*Assistant Professor, Department of Mechanical and Aerospace Engineering. Member AIAA.

†Research Associate, Department of Mechanical and Aerospace Engineering.

Mean energy conservation:

$$\frac{\partial}{\partial t}(\rho E) + \frac{\partial}{\partial x_j}(\rho u_j H) = \frac{\partial}{\partial x_j}\left[u_i \hat{\tau}_{ij} + (\mu + \sigma^* \mu_T)\frac{\partial k}{\partial x_j} - q_j\right] \tag{3}$$

Turbulent mixing energy:

$$\frac{\partial}{\partial t}(\rho k) + \frac{\partial}{\partial x_j}(\rho u_j k) = \tau_{ij}\frac{\partial u_i}{\partial x_j} - \beta^* \rho \omega k + \frac{\partial}{\partial x_j}\left[(\mu + \sigma^* \mu_T)\frac{\partial k}{\partial x_j}\right] \tag{4}$$

Specific dissipation rate:

$$\frac{\partial}{\partial t}(\rho \omega) + \frac{\partial}{\partial x_j}(\rho u_j \omega) = (\alpha \omega / k)\tau_{ij}\frac{\partial u_i}{\partial x_j} - \beta \rho \omega^2 + \frac{\partial}{\partial x_j}\left[(\mu + \alpha \mu_T)\frac{\partial \omega}{\partial x_j}\right] \tag{5}$$

where t is time, x_i position vector, u_i velocity vector, ρ density, p pressure, μ molecular viscosity, k turbulent mixing energy, and ω the specific dissipation rate. The total energy and enthalpy are $E = e + k + u_i u_i/2$ and $H = h + k + u_i u_i/2$, respectively, with $h = e + p/\rho$, and $e = p/[(\gamma - 1)\rho]$, where γ is the ratio of specific heats. The other quantities are defined in the following equations:

$$\mu_T = \alpha^* \frac{\rho k}{\omega} \tag{6}$$

$$S_{ij} = \frac{1}{2}\left[\frac{\partial u_i}{\partial x_j} + \frac{\partial u_j}{\partial x_i}\right] \tag{7}$$

$$\tau_{ij} = 2\mu_T\left[S_{ij} - \frac{1}{3}\frac{\partial u_k}{\partial x_k}\delta_{ij}\right] - (2/3)\rho k \delta_{ij} \tag{8}$$

$$\hat{\tau}_{ij} = 2\mu\left[S_{ij} - \frac{1}{3}\frac{\partial u_k}{\partial x_k}\delta_{ij}\right] + \tau_{ij} \tag{9}$$

$$q_j = -\left(\frac{\mu}{Pr_L} + \frac{\mu_T}{Pr_T}\right)\frac{\partial h}{\partial x_j} \tag{10}$$

where Pr_L and Pr_T are the laminar and turbulent Prandtl numbers, respectively. The closure coefficients are

$$\begin{aligned} &\beta = 3/40, \quad \beta^* = 9/100, \quad \alpha = 5/9 \\ &\alpha^* = 1, \quad \sigma = 1/2, \quad \sigma^* = 1/2 \end{aligned} \tag{11}$$

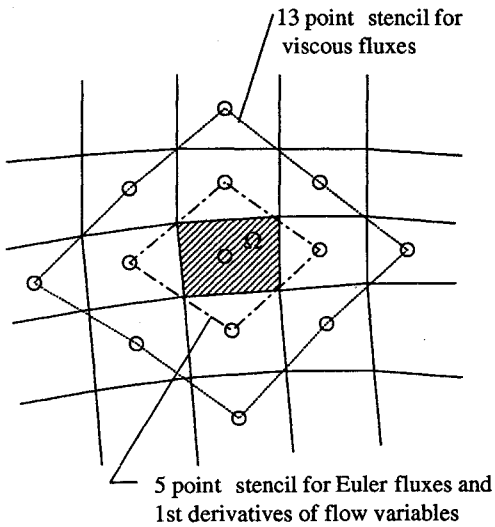

Fig. 1 Discretization stencil for the Euler flux balance, first derivatives of flow variables, and the viscous terms used in Refs. 2, 15, and 18.

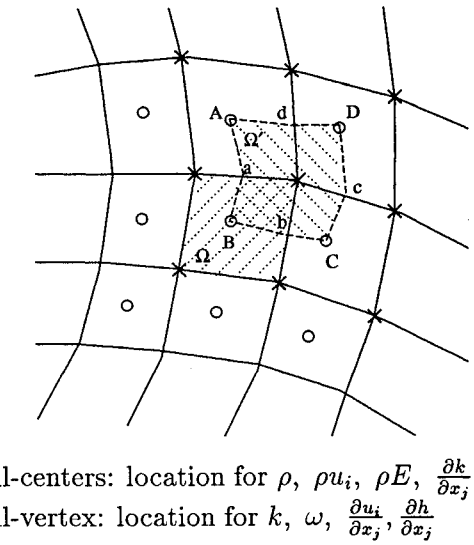

Fig. 2 Staggered control volumes for a mixed cell-center and cell-vertex scheme.

III. Numerical Method

To solve the equations described in the last section, a staggered finite volume scheme with explicit Runge-Kutta type time stepping is proposed. After the computational domain is discretized into a number of quadrilateral cells in two dimensions or hexahedral cells in three dimensions, the governing equations are applied to each of the cells in integral form. The resulting system of ordinary differential equations is then integrated in time by a hybrid multistage scheme. Residual smoothing and multigrid methods are used for the Navier-Stokes equations but are currently not implemented for the k-ω equations. The basic discretization scheme for the Navier-Stokes equations and the time integration method can be found in Refs. 1, 13, and 14. The emphasis of this paper is on the discretization of the k-ω turbulence model equations and its implications for the Navier-Stokes equations.

For simplicity, consider a computational mesh in two dimensions. With a cell-centered scheme the flow variables ρ, ρu_i, and ρE are defined at the cell centers marked by the circles in Fig. 1. Both the convective and diffusive fluxes in the Navier-Stokes equations have to be estimated over the four cell faces of a control volume, for example, the cell Ω shown in Fig. 1. The convective fluxes can be easily estimated by taking the averages of the flow variables on either side of a cell face, yielding a five-point stencil for the total Euler flux balance. Zheng and Chen,[2] Jayaram,[15] and Chen and Zheng[18] calculated the viscous stresses at each cell center by applying Gauss's formula

$$\frac{\partial u_i}{\partial x_j} \approx \frac{1}{\Omega}\int_{\partial \Omega} u_i \, \mathrm{d}s_{x_j} \tag{12}$$

where Ω is the cell volume and $\mathrm{d}s_{x_j}$ is the x_j component of the cell surface vector. The surface integration is done similarly as the convective fluxes, namely, by taking averages of the flow variables on either side of a cell face. The stencil for evaluating $\partial u_i/\partial x_j$ at the center of Ω then consists of the same five-point stencil as the Euler flux balance shown in Fig. 1. Once the stresses are known at the cell centers, the same averaging scheme can be used for calculating the diffusive fluxes. This, however, broadens the final discretization stencil for the control volume Ω since it involves extra averaging for the diffusive terms. A 13-point stencil shown in Fig. 1 will then be used.

It is known to many researchers that the aforementioned large discretization stencil not only sacrifices accuracy but also promotes spurious odd-and-even decoupling for the viscous diffusion terms. Consider the discretization of $\partial^2 u/\partial x^2 + \partial^2 u/\partial y^2$, which is the exact viscous term in the x-direction momentum equation for an

incompressible flow. It can be easily shown on a regular grid that the previous scheme allows three odd-even decoupled modes represented by the Fourier symbol: $\hat{u} = \exp(\xi l\sqrt{-1} + \eta m\sqrt{-1})$ with $(\xi, \eta) = (0, \pi)$, $(\pi, 0)$, and (π, π), where (l, m) are the grid indices in the x and y directions. It appears that these odd-even decoupled modes did not pose much difficulty in solving the Navier-Stokes equations with an algebraic turbulence model, as Zheng and Chen,[2] Jayaram,[15] and Chen and Zheng[18] all obtained good solutions for either internal or external flows. The artificial dissipation in their schemes acted to suppress the growth of the decoupled modes.

The previous scheme, however, proves to be not useful when a two-equation turbulence model is employed with the Navier-Stokes equations. First of all, if the discretization scheme is applied to the k-ω equations, the same undesirable large stencil will result. Second, and more important, if the same finite volumes are used for the k-ω equations, the resulting discrete equations lack an important coupling mechanism between the Navier-Stokes equations and the k-ω equations. We will discuss in the next few paragraphs these two problems and propose a new staggered finite volume scheme.

The appearance of a large discretization stencil in the previous scheme is because the first derivatives of velocity and temperature were defined and evaluated at the same cell center location where the flow variables are defined. In Liu and Jameson[1] a staggered auxiliary control volume Ω' was formed by connecting the cell centers A, B, C, and D and the midpoints of the cell faces a, b, c, and d as shown by the dashed lines in Fig. 2. Because the flow variables are defined at the vertices of this auxiliary cell, Eq. (12) can be applied as in a vertex scheme to calculate the velocity and temperature gradients at the center of the auxiliary cell, which in fact is the vertex of the original cell Ω. Once the stresses are known at the cell vertices of Ω, the diffusive fluxes in the Navier-Stokes equations can then be easily evaluated over the cell faces by trapezoidal rule as in a vertex scheme. This scheme that staggers the locations of the flow variables and those of their first derivatives yields a compact discretization stencil involving only nine points with minimum spatial extent as shown by the circles in Fig. 2.

It must be acknowledged, however, that the previous nine-point scheme, although being more compact, does not completely eliminate the possibility of an odd-even decoupled mode. In fact, when it is applied to the discretization of $\partial^2 u/\partial x^2 + \partial^2 u/\partial y^2$, one finds that it is still insensitive to one Fourier mode: $\hat{u} = \exp(\xi l\sqrt{-1} + \eta m\sqrt{-1})$ with $(\xi, \eta) = (\pi, \pi)$. Fortunately, we now have only one decoupled mode. In addition, this mode involves high frequencies in both x and y directions, which can be efficiently eliminated by the higher-order difference dissipation terms to be added explicitly in the Navier-Stokes equations or implicitly by upwinding in the turbulence model equations to suppress oscillations due to the convective terms in the governing equations. Boundary conditions also help suppress the growth of this two-dimensional mode. Consequently, the scheme has been found to work well in practice for the Navier-Stokes equations with either an algebraic turbulence model, as in Liu and Jameson[1] or with the two-equation turbulence model as will be shown in this paper. (The persistence of one odd-even decoupled mode in the nine-point scheme is due to the averaging of the stress tensors at the cell vertices to the center of the cell face to evaluate the viscous flux through the face. To completely eliminate the possibility of odd-even decoupling for the viscous terms, a scheme with multiple staggered sets of finite volumes similar to those used in the MAC[16] and SIMPLE[17] methods for the incompressible Navier-Stokes equations has to be used. In that case, the stress tensors ought to be evaluated directly at the center of the cell faces. Since there are more cell faces than grid points in two and three dimensions, such a scheme would generally need more computational time and storage.)

Now that we have a more compact scheme that is less prone to odd-even decoupling, we turn our attention to the more important problem, namely, the discretization of the turbulence model equations and the coupling of them with the Navier-Stokes equations. Physically, the Navier-Stokes equations and the turbulence model equations are coupled strongly through the crucial turbulent production term $\tau_{ij}(\partial u_i/\partial x_j)$ in Eqs. (4) and (5). The effect of this term on the turbulence model equations is in some sense quite similar to that of the pressure gradient in the momentum equation. It can be easily shown on a regular grid that the discretization scheme of Zheng and Chen,[2] and Jayaram,[15] and Chen and Zheng,[18] as shown in Fig. 1, uses only the center grid point and the points in the outer ring of the stencil to evaluate the viscous smoothing terms, e.g., $\partial^2 u/\partial x^2 + \partial^2 u/\partial y^2$, in the Navier-Stokes equations, whereas values of the points on the inner ring of the stencil are used to evaluate $\partial u_i/\partial x_j$ and τ_{ij}, which in turn determine the production term $\tau_{ij}(\partial u_i/\partial x_j)$ in the turbulence model equations. Evidently, two separate decoupled sets of grid points are used. The driving force of turbulent production is thus completely decoupled from the diffusive smoothing effects of the viscous terms in the Navier-Stokes equations. As a consequence, turbulent kinetic energy production may grow unsuppressed. Indeed, when such a scheme was initially attempted by the authors, persistent instability was encountered. Most of the time the instability manifested itself by an infinite growth of the turbulent kinetic energy.

With the new nine-point compact scheme we might proceed to integrate the k-ω equations using the same finite volume Ω as for the Navier-Stokes equations. If this were the case, k and ω would be defined at the cell centers, and one would have to interpolate the strain tensor calculated at the cell vertices to the cell center of Ω so that the production terms for the control volume can be evaluated. On the other hand, the eddy viscosity μ_T calculated from the k and ω at the cell centers must be translated to the cell vertices to calculate the turbulent stresses there. This double averaging process would again broaden the final discretization stencil for the coupled Navier-Stokes and the k-ω equations and thus reduce the accuracy and increase the likelihood of uninhibited growing modes.

Based on the previous analysis we propose to use the staggered control volume Ω' for integrating the k-ω equations. This time, the variables k and ω are defined not at the cell centers as marked by the circles. Rather, they are defined at the cell vertices marked by the crosses. This staggered control volume strategy, in fact, seems to be a natural way to couple the Navier-Stokes and k-ω equations. We will no longer need the excessive averaging steps for the strain tensor and the eddy viscosity. The production terms are evaluated at exactly the same locations, namely the cell vertices, where the stress and strain tensors are calculated, and the eddy viscosity calculated from the k and ω at these cell vertices is directly used to calculate the turbulent stress tensors. Again, if one draws the analogy between the significance of the pressure gradient term in the momentum equations and that of the production term in the turbulence model equations, one finds that the staggering proposed herein for the conservative flow variables and the k and ω in the turbulence model equations much resembles the staggering of the pressure and velocities used in the MAC and SIMPLE type of methods.[16,17] The velocity gradient calculated at the cell vertices with the tightest possible stencil directly drives the solution of the turbulence model equations, just as the pressure gradient calculated at a cell face directly drives the momentum equation in the MAC and SIMPLE schemes. In this way, the Navier-Stokes equations and the k-ω equations in their discrete forms are coupled as closely as possible. The discretization of each set of the equations involves a stencil of only nine points: those for the Navier-Stokes equations are shown by the circles and those for the k-ω equation by the crosses in Fig. 2.

Since the previous discretization reduces to central differencing on a regular mesh, dissipation terms of fourth-order differences need to be added to eliminate odd-and-even decoupling modes for the convective terms in regions outside the boundary layer where the grid size is too large to render the physical viscosity effective. Notice also that this dissipation term also helps eliminate the odd-even decoupling mode present in the discretization of the viscous term as discussed previously. To capture shock waves cleanly, a second difference dissipation is needed. The blended second- and fourth-order difference formulation by Jameson[13] is used for the Navier-Stokes equations. For subsonic flow the second difference dissipation is turned off completely.

A similar artificial dissipation formulation may be used for the k-ω equations. (The authors did not attempt using the artificial dissipation formulation for the k-ω equations because it seemed easier

to code an upwind scheme for the k-ω equations. However, one of the reviewers of this paper commented that central differencing with artificial dissipation for the k-ε model equations did not work.) However, it is noted that the k and ω equations have very simple wave structures that essentially consist of the convective velocities in the three coordinate directions. Therefore, upwind schemes of various orders can be easily formed based on the local convective velocity at the interface of the control volume Ω'. For instance, if the estimated normal convective velocity on the interface AaB in Fig. 2 is positive, a second-order upwind interpolation formula may be used to obtain the values k and ω at the interface midpoint a:

$$(k)_a = 1/2(3k_{l-1,m} - k_{l-2,m})$$

$$(\omega)_a = 1/2(3\omega_{l-1,m} - \omega_{l-2,m})$$

These values are then used to form the convective fluxes through the interface AaB. Higher order schemes and limiters can also be used. In this way no artificial dissipation is needed for the k-ω equations.

After space discretization, the governing equations are reduced to a set of ordinary differential equations with only derivatives in time, which can be solved by using a hybrid multistage scheme. Residual smoothing and multigrid acceleration methods are used for the Navier-Stokes equations. Details of the time-stepping scheme, residual smoothing, and multigridding can be found in Refs. 1, 13, and 14.

Though the time-stepping method is basically explicit, the source terms in the k and ω equations are treated implicitly with little additional effort. Proper evaluation of source terms is important to the stability of the computations. In the present study, the source terms are divided into two groups locally according to their sign. Only negative parts are treated implicitly. Time integrations of the Navier-Stokes and the k-ω equations are semiloosely coupled in the following fashion. A five-stage time-stepping scheme with three evaluations of the viscous terms is used for the Navier-Stokes equations (see Refs. 1, 13, and 14). The k-ω equations are marched in time separately at the first, third, and fifth stages of the five-stage time-stepping scheme when the viscous terms are evaluated. The same five-stage scheme is used for the k-ω equations. Since residual smoothing and a multigrid are used for the Navier-Stokes equations but not for the k-ω equations, it is found that the convergence of the k-ω equations usually lags behind the Navier-Stokes equations. Marching the k-ω equation four time steps within each time step for the Navier-Stokes equations greatly improves the convergence for the coupled system. In the future, a multigrid will be implemented for the k-ω equations. Different time-stepping schemes for the Navier-Stokes and the k-ω equations may also be used.

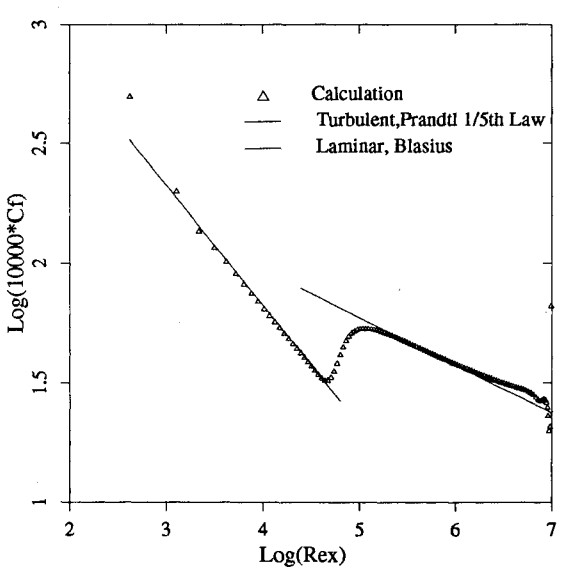

Fig. 3 Skin friction coefficient on a flat plate at $Re = 10^7$ and $M_\infty = 0.2$.

IV. Boundary Conditions

At present, H-type meshes are used. For cascade calculations we usually encounter four types of boundaries: wall, periodic, inlet, and outlet. For wall boundaries zero velocity is imposed, and the pressure is extrapolated to the wall. The turbulent mixing energy k is set to zero at the wall. The specific dissipation rate ω must satisfy the following asymptotic solution[9] as the wall is approached:

$$\omega \to \frac{6\nu_w}{\beta y^2} \tag{13}$$

as the distance $y \to 0$.

Wilcox[9] and Menter[11] used at least five mesh points within $y^+ = 2.5$ and 5, respectively. They enforced Eq. (13) at these points to achieve the proper limiting form close to the solid wall. Although this may be important for the accuracy of the near-wall velocity profile, this requirement might be stringent for flows with high Reynolds number and complex geometry. In all of our numerical examples, Eq. (13) is enforced only at the first grid point from the wall.

For periodic boundaries equivalent flow variables are imposed at corresponding cells. At the inlet boundary, the total enthalpy, total pressure, and the flow angles are specified for subsonic inlet flow. After the velocity magnitude is extrapolated from inside the flowfield, all of the flow variables on the boundary can be found. For supersonic inlet flow all flow variables are specified. Menter[12] proposed estimating the freestream values of ω by using the following equation:

$$\omega_\infty = \mathcal{O}\left(10\frac{U_\infty}{L}\right) \tag{14}$$

where U_∞ is the freestream velocity, and L is the characteristic length of the problem. The turbulent energy is specified with a small value to keep the freestream eddy viscosity at a low level. For the turbine calculations presented in the next section, the freestream k and ω are taken as $k = 10^{-6}$ and $\omega = 5$. On the outlet boundary, only the pressure is specified, and all other variables are extrapolated.

V. Computational Results

A. Low-Speed Flat-Plate Flow

Turbulent flow over a flat plate is calculated using the present method. A cascade of flat plates with a pitch-chord ratio of 2 is actually used in place of a single plate so that our computer code for cascade calculations can be used without change. Since the plates are separated two chord lengths from each other and the boundary layers are very thin, the influence on the flow over one plate by other plates may be neglected at zero angle of attack. The computation is performed on a grid of 151 × 40 with 120 cells on the plate, 24 before the leading edge, and 6 behind the trailing edge along the flow direction. Most of the first cell centers are at $y^+ = 0.5 \sim 2$ from the wall. The freestream has Mach number $M = 0.2$, Reynolds number $Re = 1 \times 10^7$, and zero angle of attack.

Figure 3 shows the calculated surface skin friction in logarithmic coordinates. It is surprising to note that the transition from laminar to turbulent flow was modeled without specifying the transition point. This was not expected without modifying the original model equations. Yet our calculations show that for whatever freestream condition with moderate μ_T, the flow remains laminar until it reaches a local Reynolds number Re_x of about 5×10^4 and becomes completely turbulent at about $Re_x = 10^5$. The computed skin friction shown in Fig. 3 agrees well with the Blasius solution in the laminar region and Prandtl's one-fifth law in the turbulent region.

B. Low-Pressure Turbine Cascade

From the previous section, it is affirmed that the k-ω model was successfully implemented and the boundary conditions were properly treated. In this section, the method is used to calculate the

flow through a low-pressure turbine cascade at its design and off-design operating conditions. This is a cascade of turbine blades with a profile typical of the root section of a low-pressure aircraft gas turbine. The cascade was extensively tested and analyzed by Hodson and Dominy.[19–21]

At its design condition this cascade has an exit isentropic Mach number of 0.7 and an incidence angle of 38.8 deg. The experimental Reynolds number based on exit velocity and blade chord length is 2.9×10^5.

The computational mesh used in the current calculations was constructed with a method developed by Chen and Zheng.[18] This method uses spring and elastic bending analogies to enforce orthogonality near blade walls. The mesh generated by this method is greatly improved over that used in Ref. 1, which was generated by an elliptic method. As shown in Fig. 4, the grid lines near the walls are nearly orthogonal. This property is very desirable for viscous calculations.

Although the blade is linear, the sidewalls have a 6-deg divergence. Therefore, a purely two-dimensional calculation would underpredict the isentropic Mach number on the forward part of the blade for the same exit Mach number. However, the divergence of the sidewalls can be easily modeled by incorporating a stream tube thickness correction in the calculation of the Euler fluxes, which has been a standard technique in cascade flow calculations. Let $h(x)$ be the stream tube area divergence ratio, which in this case varies from 1.00 at the blade leading edge to 1.06 at the blade trailing edge. The Euler portion of the Navier-Stokes equations can be modified to be

$$h(x)\frac{\partial \rho}{\partial t} + \frac{\partial \rho u h(x)}{\partial x} + \frac{\partial \rho v h(x)}{\partial y} = 0 \tag{15}$$

$$h(x)\frac{\partial \rho u}{\partial t} + \frac{\partial \rho u u h(x)}{\partial x} + \frac{\partial \rho u v h(x)}{\partial y} = -\frac{\partial p}{\partial x} + \text{viscous terms} \tag{16}$$

$$h(x)\frac{\partial \rho v}{\partial t} + \frac{\partial \rho u v h(x)}{\partial x} + \frac{\partial \rho v v h(x)}{\partial y} = -\frac{\partial p}{\partial y} + \text{viscous terms} \tag{17}$$

$$h(x)\frac{\partial \rho E}{\partial t} + \frac{\partial \rho u h(x) H}{\partial x} + \frac{\partial \rho v h(x) H}{\partial y} = \text{viscous terms} \tag{18}$$

Similar modifications in the convective terms of the k-ω equations are also made. Rigorously speaking, modifications in the viscous terms are also needed. However, since the viscous diffusion is significant only in the transverse direction rather than along the streamwise direction, neglect of the slight streamwise area change in the viscous terms has little effect on the computational results. In a finite volume scheme, the $h(x)$ factor is incorporated simply

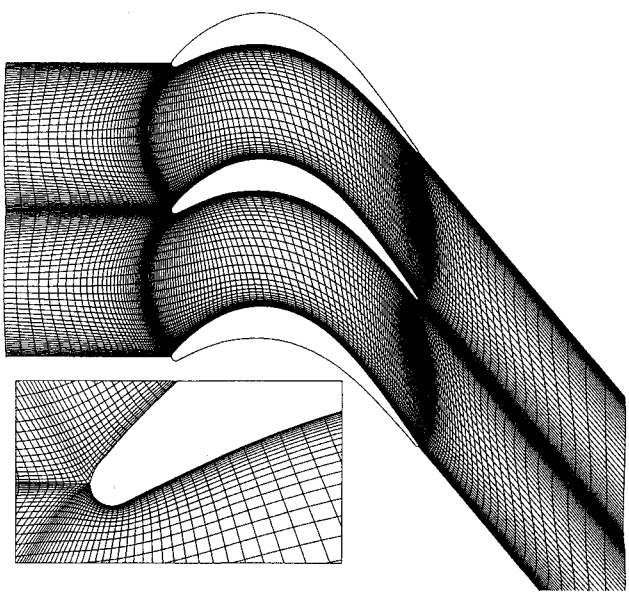

Fig. 4 160 × 48 computational grid for a turbine cascade.

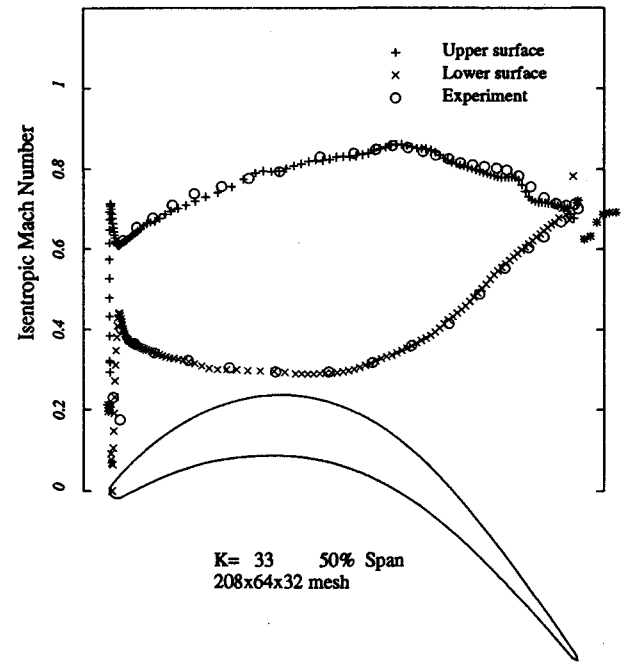

Fig. 5 Isentropic Mach number distribution at design condition, $Mis_{exit} = 0.7$, $\alpha = 38.80$ deg, and $Re = 2.9 \times 10^5$, Baldwin-Lomax model.[1]

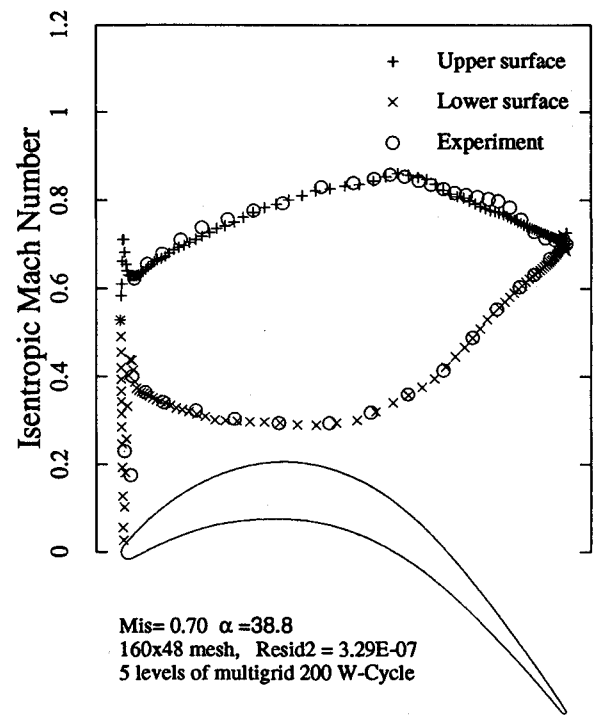

Fig. 6 Isentropic Mach number distribution at design condition, $Mis_{exit} = 0.7$, $\alpha = 38.80$ deg, and $Re = 2.9 \times 10^5$, k-ω model.

by multiplying the cell face areas by the local values of $h(x)$. Although a fully three-dimensional code has been developed, the results presented in this paper were obtained by the stripped-down two-dimensional version with the previous stream tube thickness corrections.

Liu and Jameson[1] calculated the flow for this cascade with the Baldwin-Lomax algebraic turbulence model. The computed and experimental midspan isentropic Mach number at the design condition is reproduced here in Fig. 5. Figure 6 shows the result by the present method with the k-ω turbulence model. Good overall agreement with the experimental data by Hodson and Dominy[19] is

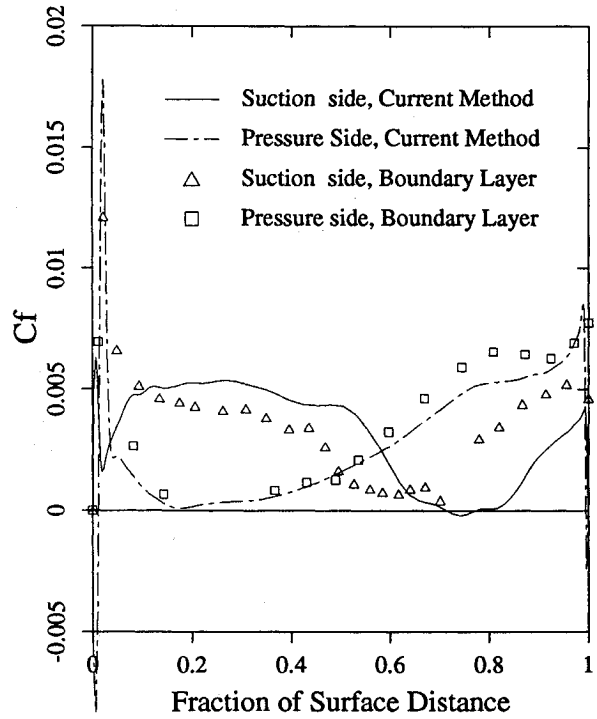

Fig. 7 Dimensionless skin friction distribution at design condition, boundary-layer solution by Ref. 19 obtained with measure Mach number distribution.

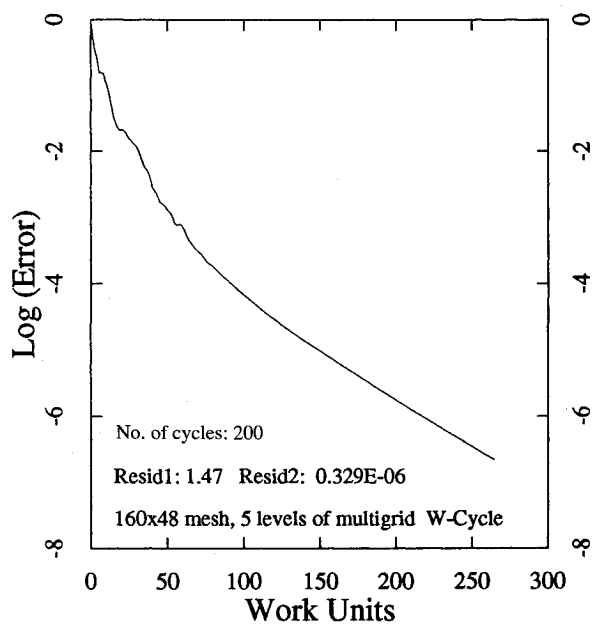

Fig. 8 Convergence history for the calculation at design condition, $M\text{is}_{\text{exit}} = 0.7$, $\alpha = 38.80$ deg, and $Re = 2.9 \times 10^5$, k-ω model.

achieved for this design operating condition. However, careful comparison between the results in Figs. 5 and 6 shows that the solution with the k-ω model misses a small hump in the isentropic Mach number distribution on the back of the suction surface. As pointed out by Hodson and Dominy,[19] the small hump was due to a laminar separation bubble. The flow becomes turbulent only after it has separated before it reattaches under the influence of turbulence. In the computation carried out in Ref. 1 with the Baldwin-Lomax model, transition was manually fixed. Zero eddy viscosity was used before the transition point, which was set at 88% axial chord location. With this manual turn-on of turbulence, the calculation successfully captured the separation bubble as observed in Fig. 5. In the current calculations with the k-ω model, the turbulent kinetic energy was set to the far-stream value before transition. It appears, however, that the transition is not as sudden as with the Baldwin-Lomax model and the separation bubble is of a smaller size so that there does not exist an obvious hump in the isentropic Mach number distribution. The calculated mass-averaged exit flow angle of this case is −53.72 deg. The experimental value is −54.1 deg.

Figure 7 shows the dimensionless skin friction distribution based on exit dynamic pressure along the blade surface as compared with the results obtained by a boundary-layer code reported by Hodson and Dominy.[19] According to Ref. 19, the boundary-layer solution was obtained by using the experimental surface Mach number dis-

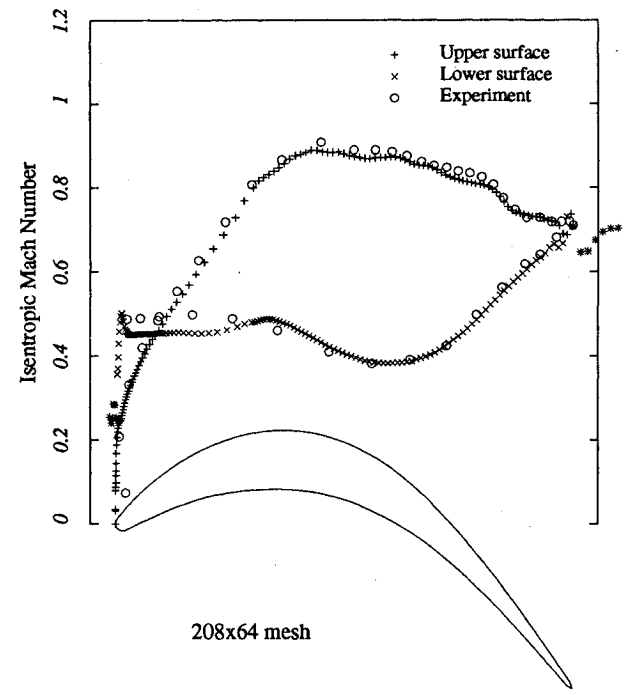

Fig. 9 Isentropic Mach number distribution at −20.3-deg incidence angle, $M\text{is}_{\text{exit}} = 0.7$, $\alpha = 18.50$ deg, and $Re = 2.9 \times 10^5$, Baldwin-Lomax model.[1]

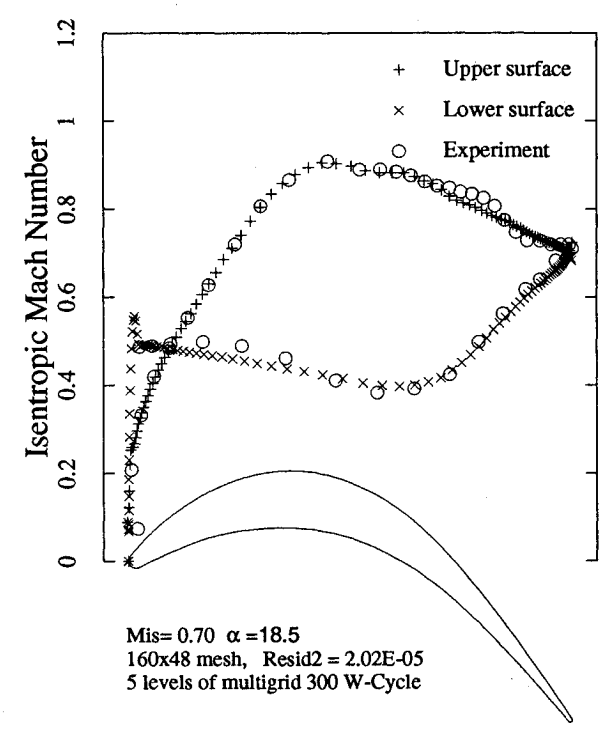

Fig. 10 Isentropic Mach number distribution at −20.3-deg incidence angle, $M\text{is}_{\text{exit}} = 0.7$, $\alpha = 18.50$ deg, and $Re = 2.9 \times 10^5$, k-ω model.

tribution as input data. Therefore one may expect that, to some extent, the boundary-layer code predictions provide a good reference for other numerical methods. The negative skin friction calculated by the current method on the suction surface between 0.7 and 0.8 fraction of surface distance indicates the existence of a small separation bubble. Although an exact match of the two solutions is not expected due to differences in turbulence and transition modeling, the agreement of the overall trend is encouraging.

Figure 8 shows the convergence history for the calculation. As mentioned in Sec. III, the multigrid is currently implemented only for the Navier-Stokes equations. The k-ω equations are solved only on the finest grid within each time stepping of the Navier-Stokes equations. Within 200 multigrid cycles for the Navier-Stokes equations, the rms residuals of density are driven to less than 1×10^{-6} as shown in Fig. 8. In fact, the solution exhibits little change after about 50 cycles. The complete calculation on a 160×48 grid with 200 cycles takes about 52 CPU min on a single processor of a Convex C-240 computer with double precision. The convergence rate for this case is the same or even faster than that with the Baldwin-Lomax model reported in Liu and Jameson.[1] Because of inaccuracies in determining the length and velocity scales, the predicted eddy viscosity by the Baldwin-Lomax model often exhibits a nonsmooth spatial distribution, particularly near regions of separation. This could hinder convergence of the Navier-Stokes calculations.

As reported in Ref. 1, a more interesting test case is the one where the incoming flow has a negative incidence angle of 20.3 deg relative to the design condition. In this case there is a large separation bubble on the pressure surface. Figure 9 reproduces a two-dimensional solution from Ref. 1 with the Baldwin-Lomax turbulence model. Although the Baldwin-Lomax model again successfully predicted the small separation bubble on the suction surface through manually setting transition (see Ref. 1), it overpredicted the size of the large separation bubble on the pressure side of the airfoil. This resulted in the significant "curving-up" of the

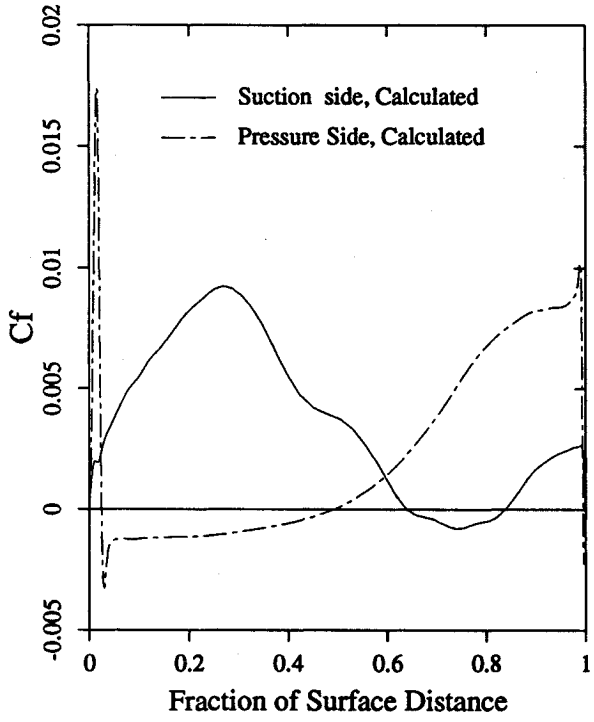

Fig. 11 Dimensionless skin friction distribution at −20.3-deg incidence angle, Mis_{exit} = 0.7, α =18.50 deg, and $Re = 2.9 \times 10^5$, k-ω model.

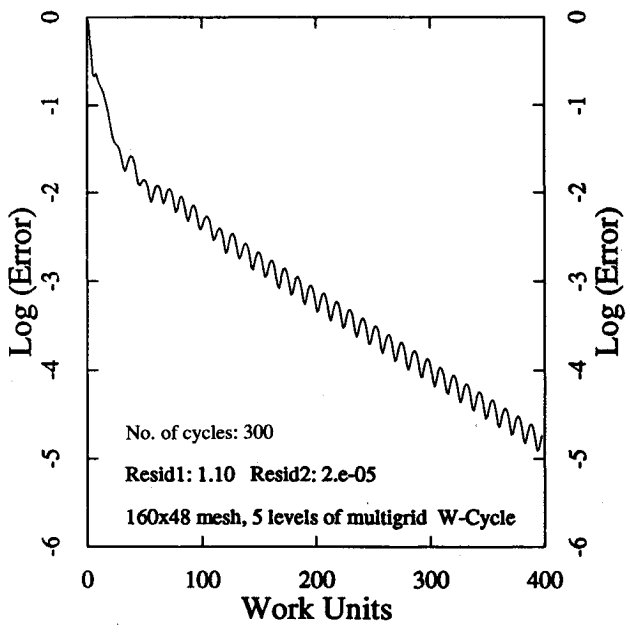

Fig. 12 Convergence history for the calculation at −20.3-deg incidence angle, Mis_{exit} = 0.7, α = 18.50 deg, and $Re = 2.9 \times 10^5$, k-ω model.

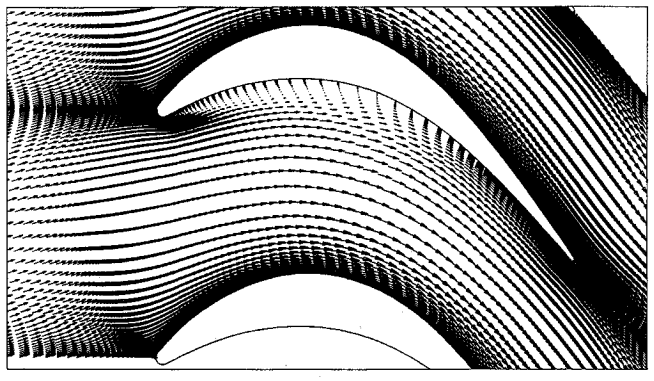

Fig. 13 Velocity vectors at −20.3-deg incidence angle, Mis_{exit} = 0.7, α = 18.50 deg, and $Re = 2.9 \times 10^5$.

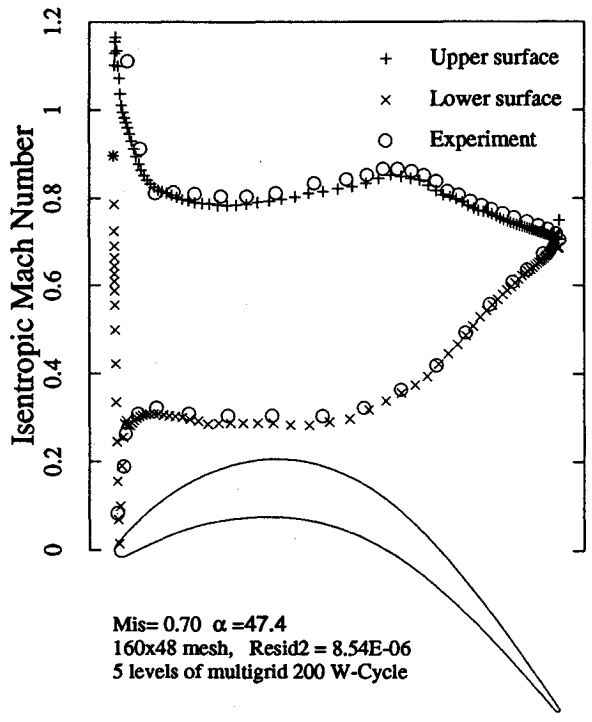

Fig. 14 Isentropic Mach number distribution at +8.6-deg incidence angle, Mis_{exit} = 0.7, α = 47.40 deg, and $Re = 2.9 \times 10^5$, k-ω model.

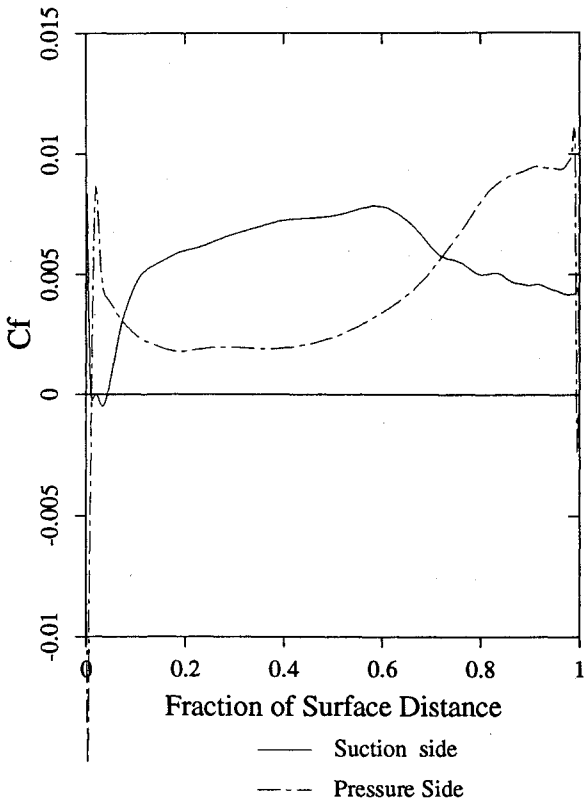

Fig. 15 Dimensionless skin friction distribution at +8.6-deg incidence angle, $M$is$_{exit}$ = 0.7, α =47.40 deg, and Re = 2.9 × 10^5, k-ω model.

isentropic Mach number distribution following the flat portion immediately after the separation. The tendency of overpredicting the separation bubble with the Baldwin-Lomax model may also have been the reason that a three-dimensional solution was not achieved in Ref. 1 since it was observed that the three-dimensional computation there exhibited unsteady oscillations of the separation region. The calculated mass-averaged exit flow angle is −53.72 deg (different from the design condition only to the third decimal place). The experimental value is −53.54 deg.

Figure 10 shows the solution by the current k-ω model. Although the calculations with the k-ω model continued to miss the small hump on the suction surface, the large separation bubble on the pressure surface was predicted with remarkably good accuracy compared with the experimental data and the solution with the Baldwin-Lomax algebraic model. There is no marked curving-up of the isentropic Mach number distribution that was evident in Fig. 9 with the Baldwin-Lomax model. Figure 11 shows the skin friction distribution over the blade, and Fig. 12 is the convergence history of the calculation for this case. The large separation zone on the pressure surface of the blade can be clearly seen. This is also confirmed by the velocity vector plot shown in Fig. 13. A boundary-layer-type calculation for this case is not possible due to the large flow separation. Compared with the design condition, this off-design condition is much more difficult because the large separation bubble on the pressure surface tends to have an unsteady behavior. The separation bubble appears to have moved very slightly during the calculation, which may account for the oscillatory character in the convergence history.

Finally, Figs. 14 and 15 show the solution at a positive 8.6-deg incidence angle relative to the design condition. Again, the calculated isentropic Mach number agrees well with experimental data. The load on the blade is greatly increased. Because of the large incidence, the flow has a small leading-edge separation bubble on the suction surface as was observed by Hodson and Dominy.[21] The computation resolved this small separation bubble that is evidenced by the skin friction distribution shown in Fig. 15. In the rear portion of the suction surface, the flow is turbulent. No flow separation was evident in either the experiments or the calculations. Thus, the isentropic Mach number distribution does not exhibit a hump of the type found in the other two operation conditions.

VI. Concluding Remarks

A staggered finite volume method for solving the Reynolds-averaged Navier-Stokes equations and the k-ω two equation turbulence model equations is presented. The method uses closely coupled compact discretization stencils for the Navier-Stokes and the k-ω equations. An explicit, multistage time-marching scheme is used to obtain steady-state solutions. The Navier-Stokes equations and the k-ω equations are loosely coupled in the time marching. A multigrid is implemented for the Navier-Stokes equations. Results show that the k-ω model without any modification predicted a transition point at about $Re_x = 5 \times 10^4$ for the flow over a flat plate at $Re_\infty = 1 \times 10^7$. Computation of the flow through a turbine cascade at its design and off-design conditions shows general agreement with the experimental data. However, the k-ω model failed to predict a small hump in the isentropic Mach number distribution on the suction surface, but calculation with the Baldwin-Lomax model was able to capture it through manually fixing a transition point based on the experimental data. On the other hand, the k-ω model was able to capture with remarkable accuracy a large separation region below the pressure surface in an off-design operating condition. Further studies will include application of multigrid methods for the k-ω equations and fully three-dimensional calculations including secondary flows.

Acknowledgments

This research was supported by the California Space Institute under Grant CS-35-92 and the Academic Senate Committee on Research at the University of California (UC), Irvine. The second author also received partial support from the Chinese National Science Foundation. Most of the computations were done on the Convex-C240 computer at UC, Irvine and the Cray Y-MP at the San Diego Super Computer Center. The authors would also like to thank the reviewers and the editor of this paper whose comments and corrections helped bring a better presentation of the contents.

References

[1]Liu, F., and Jameson, A., "Multigrid Navier-Stokes Calculations for Three-Dimensional Cascades," *AIAA Journal*, Vol. 31, No. 10, 1993, pp. 1785–1791.

[2]Zheng, X., and Chen, N., "Aerodynamic Calculation of Turbomachinery Cascade Flows with Shocks Using Euler and Navier-Stokes Solver," *Computational Mechanics*, edited by Y. K. Cheung, J. H. W. Lee, and A. Y. T. Leung, Vol. 2, Balkema/ Rotterdam/Brookfield Publication, 1991, pp. 1505–1510.

[3]Zheng, X., Zhang, M., Lai, C., Jin, H., and Zen, J., "Numerical Solution of 3D Turbulent Flows Inside of New Concept Nozzles," 18th Congress of International Council of the Aeronautical Sciences (Beijing, China), ICASE 92-3.3.3, Sept. 1992.

[4]Launder, B. E., and Spalding, D. B., "The Numerical Computation of Turbulent Flows," *Computer Methods in Applied Mechanics and Engineering*, Vol. 3, No. 2, 1974, pp. 269–286.

[5]Launder, B. E., "Phenomenological Modeling: Present and Future," *Proceedings of the Whither Turbulence Workshop*, edited by J. L. Lumley, Vol. 357, Lecture Notes in Physics, Springer-Verlag, Berlin, 1990, pp. 439–485.

[6]Speziale, C. G., "Analytical Methods for the Development of Reynolds Stress Closures in Turbulence," *Annual Review of Fluid Mechanics*, Vol. 23, 1991, pp. 107–157.

[7]Patel, V. C., Rodi, W., and Scheuerer, G., "Turbulence Models for Near-Wall and Low Reynolds Number Flows: A Review," *AIAA Journal*, Vol. 23, No. 9, 1985, pp. 1308–1319.

[8]Speziale, C. G., Abid, R., and Anderson, E. C., "Critical Evaluation of Two-Equation Models for Near-Wall Turbulence," *AIAA Journal*, Vol. 30, No. 2, 1992, pp. 324–331.

[9]Wilcox, D. C., "Reassessment of the Scale-Determining Equation for Advanced Turbulence Models," *AIAA Journal*, Vol. 26, No. 11, 1988, pp. 1299–1310.

[10]Wilcox, D. C., "A Half Century Historical Review of the k-ω Model," AIAA Paper 91-0615, Jan. 1991.

[11]Menter, F. R., "Performance of Popular Turbulence Models for Attached and Separated Adverse Pressure Gradient Flows," AIAA Paper 91-

1784, June 1991.

[12]Menter, F. R., "Influence of Freestream Values on k-ω Turbulence Model Predictions," *AIAA Journal,* Vol. 30, No. 6, 1992, pp. 1657–1659.

[13]Jameson, A., "Transonic Flow Calculations," Dept. of Mechanical and Aerospace Engineering, Princeton Univ., MAE Rept. 1651, Princeton, NJ, July 1983.

[14]Liu, F. "Numerical Calculation of Turbomachinery Cascade Flows," Ph.D. Thesis, Dept. of Mechanical and Aerospace Engineering, Princeton Univ., Princeton, NJ, June 1991.

[15]Jayaram, M., "Solutions of the Three-Dimensional Navier-Stokes Equations for Transonic Flow Using a Multigrid Method," Ph.D. Thesis, Dept. of Mechanical and Aerospace Engineering, Princeton Univ., Princeton, NJ, 1987.

[16]Harlow, F. H., and Welch, J. E., "Numerical Calculation of Time-Dependent Viscous Incompressible Flow of Fluid with Free Surface," *Physics of Fluids,* Vol. 8, No. 12, 1965, pp. 2182–2189.

[17]Patanka, S. V., *Numerical Heat Transfer and Fluid Flow,* Hemisphere, Washington, DC, 1980.

[18]Chen, N., and Zheng, X., "Numerical Computations of Turbomachinery Cascade Turbulent Flows Using a Multigrid Scheme," 18th Congress of International Council of the Aeronautical Sciences, ICASE 92-3.1.3, Beijing, China, Sept. 1992.

[19]Hodson, H. P., and Dominy, R. G., "Boundary Layer Transition and Separation Observed near the Leading Edge of a High Speed Turbine Blade," *ASME Journal of Engineering for Gas Turbines and Power,* Vol. 107, No. 1, 1985, pp. 127–134.

[20]Hodson, H. P., and Dominy, R. G., "Three-Dimensional Flow in a Low Pressure Turbine Cascade at its Design Condition," *ASME Journal of Turbomachinery,* Vol. 109, No. 2, 1987, pp. 177–185.

[21]Hodson, H. P., and Dominy, R. G., "The Off-Design Performance of a Low Pressure Turbine Cascade," *ASME Journal of Turbomachinery,* Vol. 109, No. 2, 1987, pp. 201–209.

MARS: PAST, PRESENT, AND FUTURE

E. BRIAN PRITCHARD, EDITOR

AIAA Progress in Astronautics and Aeronautics Series
1992, 332 pp, illus, ISBN 1-56347-043-8
AIAA Members $49.95 Nonmembers $69.95 • Order #: V-145(830)

This new edition contains the excellent invited papers presented at the Mars Exploration: Past, Present, and Future Conference, July 1991. Of particular interest are the papers on the Viking mission. They provide valuable management lessons learned for future program and project managers. Twenty-eight chapters are divided into six parts: Overviews; Prior Missions; Future Missions: Rationale and Benefits; Future Missions: Robotic Missions; Future Missions: Systems Concepts and Operations; Future Missions: Technology

Place your order today! Call 1-800/682-AIAA

AIAA

American Institute of Aeronautics and Astronautics

Publications Customer Service, 9 Jay Gould Ct., P.O. Box 753, Waldorf, MD 20604
FAX 301/843-0159 Phone 1-800/682-2422 8 a.m. - 5 p.m. Eastern

Sales Tax: CA residents, 8.25%; DC, 6%. For shipping and handling add $4.75 for 1-4 books (call for rates for higher quantities). Orders under $100.00 must be prepaid. Foreign orders must be prepaid and include a $20.00 postal surcharge. Please allow 4 weeks for delivery. Prices are subject to change without notice. Returns will be accepted within 30 days. Non-U.S. residents are responsible for payment of any taxes required by their government.